




Ambient PM2.5 exposure causes cellular senescence via DNA damage, micronuclei formation, and cGAS activation

Tao Wu, Shengmin Xu, Biao Chen, Lingzhi Bao, Jie Ma, Wei Han, An Xu, Kwan Ngok Yu, Lijun Wu & Shaopeng Chen


To cite this article: Tao Wu, Shengmin Xu, Biao Chen, Lingzhi Bao, Jie Ma, Wei Han, An Xu, Kwan Ngok Yu, Lijun Wu & Shaopeng Chen (2022) Ambient PM2.5 exposure causes cellular senescence via DNA damage, micronuclei formation, and cGAS activation, *Nanotoxicology*, 16:6-8, 757-775, DOI: [10.1080/17435390.2022.2147460](https://doi.org/10.1080/17435390.2022.2147460)

To link to this article: <https://doi.org/10.1080/17435390.2022.2147460>

 View supplementary material [↗](#)

 Published online: 20 Nov 2022.

 Submit your article to this journal [↗](#)

 Article views: 80



 View related articles [↗](#)

 View Crossmark data [↗](#)

ARTICLE



Ambient PM_{2.5} exposure causes cellular senescence via DNA damage, micronuclei formation, and cGAS activation

Tao Wu^{a,b}, Shengmin Xu^c, Biao Chen^a , Lingzhi Bao^d, Jie Ma^d, Wei Han^a, An Xu^a, Kwan Ngok Yu^{e,f}, Lijun Wu^{a,c} and Shaopeng Chen^{a,d} 

^aHigh Magnetic Field Laboratory, Key Laboratory of High Magnetic Field and Ion Beam Physical Biology, Hefei Institutes of Physical Science, Chinese Academy of Sciences, Hefei, China; ^bUniversity of Science and Technology of China, Hefei, China; ^cInformation Materials and Intelligent Sensing Laboratory of Anhui Province, Institutes of Physical Science and Information Technology, Anhui University, Hefei, China; ^dSchool of Public Health, Wannan Medical College, Wuhu, China; ^eDepartment of Physics, City University of Hong Kong, Hong Kong, China; ^fState Key Laboratory in Marine Pollution, City University of Hong Kong, Hong Kong, China

ABSTRACT

Ambient PM_{2.5} is one of the environmental risk factors and was correlated with senescence-related diseases based on the epidemiologic investigation. However, little is known about senescence induced by PM_{2.5} as well as the underlying mechanisms. In this study, we demonstrated that PM_{2.5} exposure aggravated cellular senescence *in vivo* and *in vitro*, and disrupted micronuclei (MN) played a vital role in this process. Our results suggested that the nuclear envelope (NE) of PM_{2.5}-induced MN was ruptured. Subsequently, cGAS was found to localize to approximately 80% of the disrupted MN but few for intact MN. Upon examination of cGAMP and SA-β-Gal, the cGAS-STING pathway was found activated and related to cellular senescence induced by PM_{2.5}. Taken together, we reported a novel finding that PM_{2.5} exposure causes cellular senescence *via* DNA damage, MN formation, and cGAS activation. These results revealed the potential toxicity of PM_{2.5} and its related mechanisms in cellular senescence.

Abbreviations: NE: Nuclear envelope; MN: Micronuclei; HLF: Human lung fibroblast; cGAS: Cyclic GMP–AMP synthase; SASP: Senescence-associated secretory phenotype; cGAMP: cyclic GMP–AMP

ARTICLE HISTORY

Received 21 July 2022
Revised 10 October 2022
Accepted 9 November 2022

KEYWORDS

PM_{2.5}; senescence; cGAS; micronuclei; DNA damage


1. Introduction

Environmental pollutants have been a rising global threat and burden to human health for many decades, especially in developing countries (Forouzanfar et al. 2016; Araviiskaia et al. 2019). Among various air pollutants, particulate matter ([PM_{2.5}], particle size ≤ 2.5 μm) is the most harmful component consisting of organic matter, metal, dust, and liquid droplets (Abbas et al. 2013; Peng et al. 2019). Epidemiological studies have recently shown an association between ambient PM and senescence-related diseases, including idiopathic pulmonary fibrosis (IPF) and chronic obstructive pulmonary disease (COPD) (Schuliga et al. 2020; Yang, Li, and Tang 2020; Tahara et al. 2021). However, the effects of PM_{2.5} exposure on cellular senescence are not well understood.

Cellular senescence is known as a stress-induced irreversible cell cycle arrest which is characterized by complex characteristics, such as cytokine secretion disorder, expression of senescence associated-beta-galactosidase (SA-β-Gal), and dysregulated protein expression (Kamal et al. 2020; Wang, Chen, and Cai 2021). Senescence occurs when mitotic progression is progressively interrupted following genomic instability, especially double-strand breaks (DSBs) (Van Deursen 2014; Ogrodnik et al. 2019). Meanwhile, senescent cells are more abundant in aged and diseased tissues, driving a large number of age-related pathologies including atherosclerosis and pulmonary fibrosis (Baker et al. 2016; Childs et al. 2016; Demaria et al. 2017).

Cyclic GMP–AMP synthase (cGAS) is known as a cytosolic DNA sensor, and is essential for cellular senescence (Yang et al. 2017). Through cyclic GMP–

CONTACT Shaopeng Chen  20200080@wnmc.edu.cn  High Magnetic Field Laboratory, Key Laboratory of High Magnetic Field and Ion Beam Physical Biology, Hefei Institutes of Physical Science, Chinese Academy of Sciences, Hefei, PR China

 Supplemental data for this article can be accessed online at <https://doi.org/10.1080/17435390.2022.2147460>

© 2022 Informa UK Limited, trading as Taylor & Francis Group

AMP (cGAMP) synthesis, stimulator of interferon genes (STING) can be activated, and it upregulates type I IFNs and the interferon-stimulated gene (ISG), which gives rise to senescence-associated secretory phenotype (SASP) and cellular senescence (Ablasser et al. 2013; Li and Chen 2018). Deletion of cGAS can also terminate the cellular senescence and SASP caused by DNA-damaging factors (Yang et al. 2017). Micronuclei (MN) is a small segment of a chromosome without a centromere after cell division, and DNA in the MN is tightly segregated within the nucleus by the nuclear membrane (Hintzschke et al. 2017). Recent studies found that self-DNA in the MNs can be surveyed by cGAS, leading to the activation of subsequent inflammatory signal pathways (Mackenzie et al. 2017). In addition, PM_{2.5} exposure inhibited the integrin signaling pathway, causing DNA damage, and MNs formation (Longhin et al. 2013; Di Domenico et al. 2020; Song et al. 2022). Based on the function of cGAS in cellular senescence and the findings that PM_{2.5} exposure causes DNA damage, MNs formation and inflammatory response, etc., we speculated that PM_{2.5}-induced cellular senescence was associated with DNA damage, MN formation, and cGAS activation.

To prove our hypothesis, C57 mice and primary human-derived lung fibroblasts were exposed to ambient PM_{2.5} from Taiyuan, a typical seriously polluted city in China for energy production, chemical and coal combustion industries. In this work, we showed that PM_{2.5} exposure caused cellular senescence in the lung cells both *in vivo* and *in vitro*, and this process was connected to MNs formation. Disrupted MNs by PM_{2.5} exposure, in which cGAS accumulated, triggered the cGAS-STING pathway and contributed significantly to cellular senescence. As a result, we identified a novel toxic effect of PM_{2.5} on lung fibroblasts as well as the mechanism of PM_{2.5} on cellular senescence, and these findings provide alternative perspectives on the health impacts of PM_{2.5}.

2. Materials and methods

2.1. Sample preparation and characterization

The PM_{2.5} was given by Sang, and was collected in the winter of 2016. By soaking the filter in deionized water for 30 min, vortexing it for 5 min, and

then sonicating it, the PM_{2.5}-containing filter was converted to an aqueous suspension (30 min). In order to better understand the real toxicity of PM_{2.5}, the blank quartz filter membrane was vortexed and sonicated as same as the PM_{2.5} sample. Then the filter group after being freeze-dried was also dissolved with PBS and used as the control group. PM_{2.5} dissolved in water was freeze-dried to form PM_{2.5} powder and then dissolved with PBS (containing 100 U/mL penicillin and streptomycin) to the required concentration. Before treating cells or mice, the samples needed to be vortexed and sonicated for 15 min again. The part of metal contents in PM_{2.5} samples was determined by inductively coupled plasma-mass spectrometry (ICP-MS).

2.2. Isolation and culture of human lung fibroblasts (HLF)

Primary lung fibroblasts were isolated from the male human lung tissue who was undergoing surgery. Ethical approval was given by the Institutional Animal Care and Use Committee of Hefei Institutes of Physical Science, Chinese Academy of Sciences (Reference number: SWYX-Y-2021-10). Informed consent was obtained. The lung fibroblasts were isolated according to previously reported protocols (Seluanov et al. 2008). Briefly, following two PBS washes to remove the erythrocyte, the lung tissues were immediately cut into tiny pieces and digested with trypsin for 10 min in the incubator. After being centrifuged for 3 min, the digested tissues were plated onto 10-cm dishes with DMEM (Gibco, Waltham, MA) supplemented with 10% (v/v) FBS (Bio-west, Nuaille, France) and 1% (v/v) penicillin-streptomycin (Gibco). Digested tissues were then maintained in the incubator and after 12 h of culture, 80% of adherent cells were lung fibroblasts. The cells were regularly passaged at 70–80% confluent, and the 4th–12th generations of the cells were used for subsequent experiments.

The isolated human lung fibroblasts (HLFs) were grown in DMEM medium with 10% fetal bovine serum (Bio-west, Nuaille, France), 100 U/mL penicillin and streptomycin (Beyotime, Haimen, China) in an incubator (95% humidity and 5% CO₂ at 37 °C).

2.3. PM2.5 exposure

Fibroblasts were randomly assigned to treatment groups that prepared PM2.5 at doses of 25, 50, 75, and 100 $\mu\text{g}/\text{mL}$ and control groups that were incubated exclusively in DMEM.

The male mice (C57BL/6) used in the study were approximately six weeks old and housed under standard conditions. Considering realistic PM2.5 exposures, we treated mice with dosages of 1 and 5 mg/kg bw (body weight [bw]) every 2 d for 4 weeks. Mice were treated with PM2.5 and controlled by intratracheal instillation. All of the mice included in the experiment had unrestricted access to food and water. The Institutional Animal Care and Use Committee of Hefei Institutes of Physical Science, Chinese Academy of Sciences, authorized all procedures (Laboratory Animal Facility License Number: SYXK-2019-010).

2.4. Real-time quantitative reverse transcription-PCR

Total RNA was extracted using Trizol Reagent (Invitrogen, Waltham, MA) in accordance with the manufacturer's instructions, and a reverse transcription kit was used to create complementary DNA (cDNA) from the extracted total RNA (Transgene, Beijing, China). According to the manufacturer's instructions, the SYBR Green PCR Kit (Transgene, China) materials were mixed together and the RT-PCR with specified primers was performed by a Real-Time PCR machine (Lightcycler 96, Roche, Basel, Switzerland). The RT-qPCR reaction settings were as follows: after 15 min at 95 °C, 40 cycles with annealing temperatures of 58 °C and 55 °C for 20 s each were run, followed by 30 s at 72 °C. In the Supporting Information (SI), Table S1 lists the primer sequences.

2.5. Western blotting

The treated cells were centrifuged at 12,000 *g* for 15 min before being rinsed with ice-cold PBS and extracted by scraping in ice-cold lysis buffer. Prior to resolution through sodium dodecyl sulfate (SDS)-polyacrylamide gel electrophoresis (PAGE), the concentration of total protein was measured using a BCA Protein Assay Kit from Thermo, China. A PDVF membrane was used to transfer 30 μg of total

protein, which was then blocked with 5% bovine serum albumin (BSA). The membrane was first incubated with the primary antibody at 4 °C for an overnight period, followed by an hour at room temperature with the secondary antibody. According to the instructions, the following primary antibodies and complementary secondary antibodies (1:10,000) were used (Supplementary Table 2). Tanon-5200 (Tanon-5200, Shanghai, China) Imager and Image Lab Software were used to photograph the proteins of interest and the enhanced chemiluminescence substrate ECL to detect them.

2.6. Immunofluorescence

Fibroblasts were grown on coverslips after being exposed to PM2.5, and they were then fixed with 4% paraformaldehyde (PFA) for 10 min, permeabilized with PBST (PBST includes 0.5% Triton X-100), and blocked with 5% BSA in PBST for 1 h at room temperature. The primary antibody was incubated with the cells in PBST containing 5% BSA for 1 h. Cells were incubated with the secondary antibody in PBST for 1 h after being washed with PBST three times. Before the cells were coverslipped in a fluorescence protection agent, they were counterstained for 10 min with Hoechst 33342. The images were taken with a fluorescence microscope (Leica DM4B, Wetzlar, Germany).

2.7. SA- β -galactosidase staining

The endogenous lysosomal enzyme senescence-associated β -galactosidase (SA- β -gal) is an important biomarker for senescence tracking and senescent cells often exhibited overexpression of SA- β -Gal (Kamal et al. 2020). According to the manufacturer's instructions, a senescence staining kit (Solarbio, Beijing, China) was applied to detect cellular senescence. Cells were rinsed in 1 mL of ice-cold PBS, fixed for 10 min with 3 mL of 1% PFA at room temperature, and then washed once with PBS. Then the cells were reconstituted in 2 mL of freshly made staining solution, and they were incubated horizontally for 24 h at 37 °C while being shielded from light and CO₂. All the images were captured using a fluorescence microscope (Leica DM4B, Germany) after cells were counterstained with Hoechst 33342 for 10 min. The sections (5 μm)

of tissues were stained in SA-Gal staining solution without CO₂ for a whole night before being seen in bright field.

2.8. Cell cycle detection by flow cytometry

Trypsin was used to separate the cells into single cell after washing them with ice-cold PBS. The cells were then fixed with 75% ethanol solution for an overnight period, washed twice in ice-cold PBS, and stained for 30 min with 50 g/mL Propidium Iodide (PI) containing 100 g/mL RNase. From the total of 2×10^4 cells, the cell cycle was examined using FACScan BD (Becton Dickinson Biosciences, Franklin Lakes, NJ).

2.9. Determination of micronucleus frequency

Micronucleus frequency was assessed using microscopy after the cells had been fixed with 4% PFA and stained with Hoechst 33342. The apoptotic appearance was discarded, and MN were classified as distinct DNA clumps isolated from primary nuclei.

2.10. Histology and immunohistochemistry

After being collected, the lung tissues of mice were fixed in 4% PFA and then embedded in paraffin blocks. Hematoxylin-eosin (H&E) staining and Masson staining of tissue sections (5 μm) were carried out according to protocol. Sections were submerged in 10 mM sodium citrate (pH 6.0) at 95 °C for 30 min to perform antigen retrieval prior to immunohistochemical labeling. The primary human cGAS antibodies (1:200, Cell Signaling Technology, Danvers, MA) were then applied to the sections and incubated at 4 °C for an overnight period. The degree of peribronchial and perivascular inflammation was scored from 0 to 10 using the following criteria: 0, normal; 1–4, mild; 5–6, moderate; 7–8, severe; 9–10, very severe. Masson staining was used to determine collagen deposition around bronchi and scores from 0 to 3 were applied: 0–1, no or little collagen around bronchi; 1–2, a thin layer of collagen deposition; 2–3, a cluster or a thick layer of collagen deposition. The expression of α-SMA in the mice lung tissue was quantified by using Image software.

2.11. siRNA knockdown

After an overnight incubation, cells were plated at the appropriate density (2.0×10^5 fibroblasts per 60 mm dish) and transfected with siRNA oligonucleotides targeting cGAS at a final concentration of 10 nM the next day. Hiperfect (QIAGEN, Hilden, Germany) transfections were carried out in accordance with the manufacturer's instructions, in DMEM with 10% serum medium (Gibco, Waltham, MA). siRNA targeting cGAS (sense, 5'-GCUGAACACUUCUUAUUA-3') was synthesized from GenePharma (Shanghai, China).

2.12. EDU assay

The fibroblasts were incubated in DMEM with 10 μM EdU for 2 h following PM2.5 exposure and nuclei were counterstained with Hoechst 33342. Then cells were analyzed using a Click-iT EdU Assay Kit from Invitrogen. The images of cells positive for EdU were captured randomly by microscopy.

2.13. Cell proliferation assay

Using a CCK8 Cell Proliferation Kit I (Sigma-Aldrich, St. Louis, MO), cell viability was indirectly evaluated. Fibroblasts were treated with PM2.5 in the 96-well cell culture plate for 3 d and the CCK8 reagent was added to the plate for 10 μL per well. After 1 h incubated in an incubator, quantification was performed with a spectrophotometer.

2.14. CGAMP ELISA assay

Commercial kits (Cyclic GAMP (cGAMP) ELISA, Arbor Assays, Ann Arbor, MI) were used in accordance with the manufacturer's instructions to perform specific sandwich enzyme-linked immunosorbent assays (ELISA) to quantify the concentrations of cGAMP in cell supernatants.

2.15. Enzyme activity inhibition of cGAS

RU.521 is a potent and selective cGAS inhibitor and inhibits cGAS-mediated interferon upregulation. The activation of cGAS requires the involvement of dsDNA. RU.521 suppresses cGAS activity by interfering with its association with dsDNA through binding to the catalytic pocket of cGAS competitively

and inhibits its dsDNA-stimulated activity. The cGAS small-molecule inhibitors RU.521 (Topscience, Shandong, China) were prepared as 20 mM stocks in 100% dimethyl sulfoxide (DMSO). The cells were incubated overnight and inhibitors were added to the concentration of 700 nM accompanied by PM2.5 exposure.

2.16. Generation of GFP-cGAS cell lines

GFP-cGAS expressing plasmid (pTRIP-CMV-GFP-FLAG-cGAS) was purchased from Addgene (#86675). To generate viral particles, the resulting pTRIP vectors and packaging vectors (pMD2.G, psPAX2) were transfected into 293 T cells using polyethyleneimine (PEI), a kind of transfection reagent capable of gene transfection *in vitro*. After 24 h culture; we collected the supernatant of the medium. In the presence of 1 µg/mL polybrene, the supernatant was used to infect the fibroblasts. After infection, the cells expressing cGAS-GFP were identified by flow cytometry.

2.17. DNA repair assays

The Homologous recombination (HR) and nonhomologous end joining (NHEJ) reporters are based on an engineered GFP gene containing recognition sites for I-SceI endonuclease for induction of DSBs (Seluanov, Mao, and Gorbunova 2010). The reporters are GFP negative due to an additional exon that existed in the GFP sequence. Successful repair of the I-SceI-induced breaks by NHEJ or HR reconstructs the functional GFP gene. The number of GFP-positive cells is counted by flow cytometry, providing a quantitative efficiency of NHEJ and HR. Human embryonic kidney epithelial cells (293 T) cells were seeded at 1×10^5 cells in a 35 cm dish and were cultured for 24 h. The cells were transfected with 2 µg of I-SceI (to induce DSBs), 0.2 µg of mCherry (as a reference internally to assess transfection effectiveness) and 1 µg of HR and NHEJ reporter. PM2.5 exposures were performed 6 h after transfection for 3 d. Fluorescence-activated cell sorting (FACS) was used to examine the effectiveness of DSB repair using a BD FACSVerse (BD Biosciences, Franklin Lakes, NJ). The ratio of GFP⁺ cells and mCherry⁺ cells was used to calculate the efficiency of HR and NHEJ. More than 10,000 cells

were counted. The operation of transfection was processed *via* lipofectamine 2000 transfection reagent (Invitrogen). Experiments were performed in triplicates.

2.18. Transmission electron microscopy (TEM) observation

Mice's lung tissues were dried, dyed en bloc, fixed with 2.5% glutaraldehyde, and embedded in beam capsules. Following that, copper grids were used to harvest 100 nm-thick sections of the implanted tissue, which were then stained with uranyl acetate and lead citrate. For observation, a transmission electron microscope (Talos F200X, Houston, TX) was utilized.

2.19. Statistical analysis

The results of all quantitative *in vitro* tests are shown as the mean ± SEM of three separate tests, and the results of *in vivo* tests are shown as the mean ± SD of more than three mice per group. The PM2.5 treatment and control groups were compared using an unpaired, two-tailed Student's t-test with a *p* value < 0.05 considered statistically significant and two-way ANOVA followed by Student's t-test was used for time and dosage-dependent experiments using the GraphPad Prism version 8.0 (GraphPad Software, Graphpad Software Inc., La Jolla, CA). When *p* < 0.05, differences in all tests were considered significant.

3. Results

3.1. PM2.5 exposure aggravates lung cellular senescence *in vivo*

PM2.5 samples in this study were collected from Taiyuan, a coal hub in Northern China, using quartz filters (Figure S1(A)). The average particle size of the PM2.5 sample was measured through a particle sizing system (Malvern Zetasizer Nano ZSE, Malvern, UK) and the size distribution (< 2.5 µm) was consistent with the definition of PM2.5 (Figure S1(B)). The metal component in the PM2.5 samples were assayed by ICP-MS and the component distribution are shown in Figure S1(C,D).

To explore whether PM2.5 induces lung cellular senescence *in vivo*, 1 and 5 mg/kg bw PM2.5 were

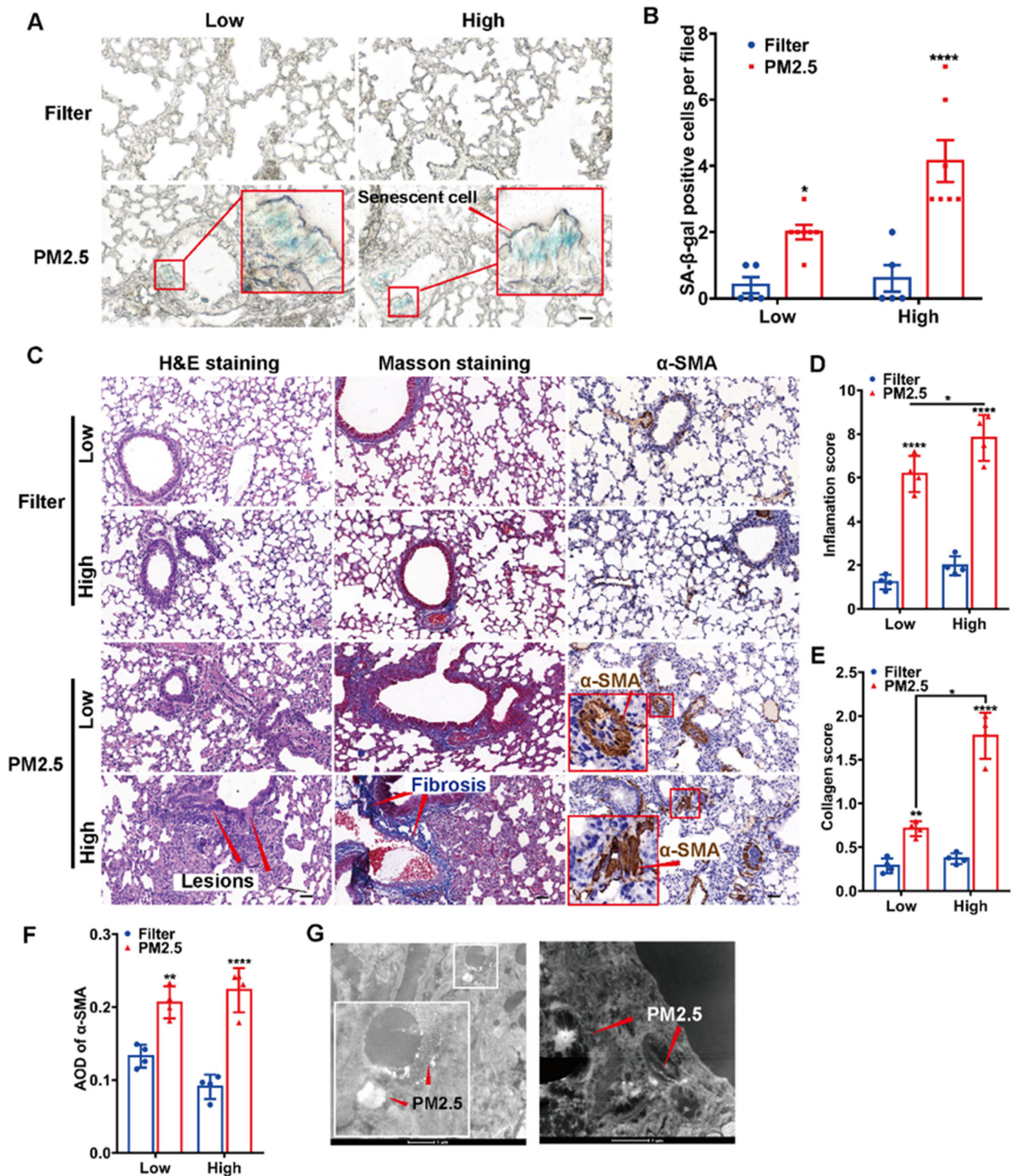


Figure 1. PM2.5 exposure induced lung cellular senescence and related phenotypes in C57BL/6 mice. (A) Senescent cells in the lung tissue section were identified with SA-β-gal staining (bw: bodyweight, scale bar: 50 μm). Mice were treated with PM2.5 at 1 (Low) and 5 (High) mg/kg bw for 4 weeks. 'Low' and 'High' represent respectively indicate that the treatment concentrations of PM2.5 in mice of 1 and 5 mg/kg bw, respectively. (B) Quantification of SA-β-gal positive cells per field in section of lung tissue. (C) Histological examination of mice lungs. Tissue sections were stained with H&E, Immunohistochemistry (IHC) (examination of α-SMA), and Masson's Trichrome (scale bar: 50 μm). (D, E) Quantitative analysis of H&E and Masson staining. (F) Quantitative analysis of α-SMA using Image software. AOD: average optical density. (G) Image of residual PM2.5 in lung tissues of mice following the exposure taken by TEM, with red arrows indicating residual PM2.5 in lung tissue. These data for *in vivo* experiment are expressed as the mean ± SD, $n = 4-5$ mice per group, * $p < 0.05$, ** $p < 0.01$, and **** $p < 0.0001$ compared with filter group by using two-way ANOVA.

exposed to mice every 2 d for 4 weeks. After exposure, the mice were sacrificed and the lungs were cut for tissue section (5 μm). The results of β -galactosidase staining showed that PM2.5 aggravated lung cellular senescence of mice, with more severe senescence at 5 mg/kg bw group (Figure 1(A,B)). Additionally, H&E staining of the mice lungs revealed that PM2.5 induced significant pulmonary inflammation (Figure 1(C,D)). We observed that PM2.5-treated mice presented inflammatory cell infiltration in the peribronchial areas, alveolar lesions and damage, and tracheobronchial wall thickening (as arrows indicated) (Figure 1(C)). In the meantime, mice exposed to PM2.5 showed a tendency of lung fibrosis at 5 mg/kg bw, according to the results of Masson staining and α -SMA (alpha smooth muscle actin, used as indications of pulmonary fibrosis) labeling (Figure 1(C,E,F)). Peribronchial collagen deposition was also observed in PM2.5-treated group (The blue area where indicated by the arrow) (Figure 1(C)). Meanwhile, the expression level of α -SMA (brown area as arrows indicated) around the parabronchial areas in the treatment group was higher compared with the filter group (Figure 1(C)). Importantly, all the alterations in the study from the 'High' group were more significant than those in the 'Low' groups. In addition, the images taken by TEM also showed that PM2.5 remained and deposited in the lungs of mice (Figure 1(G)). These results suggested that PM2.5 exposure induced lung cellular senescence, inflammation, and fibrosis *in vivo* depending on the dose of PM2.5 exposure.

3.2. PM2.5 exposure aggravates lung fibroblasts senescence *in vitro* in a dose and time-dependent manner

To access the effects of PM2.5 on lung fibroblasts senescence *in vitro*, we examined SA- β -Gal activity of PM2.5 exposed fibroblasts through β -X-Gal staining. Compared with the filter group, PM2.5 induced fibroblasts senescence significantly in a time (3 and 9 d, 100 $\mu\text{g}/\text{mL}$) and dosage (25, 50, 75, and 100 $\mu\text{g}/\text{mL}$, 3 d) dependent manner (Figure 2(A–C)). The result of EdU assay showed that PM2.5 exposure caused decreased cell proliferation according to the fewer EdU positive cells (Red) in PM2.5 treated group (Figure 2(D,E)). The result of CCK-8 assay

(Figure 2(F)) indicated that the cell viability decreased significantly after PM2.5 exposure. With further cell cycle analysis, we demonstrated that PM2.5 exposure caused cell cycle arrest at G1 phase (Figure 2(G)). Moreover, we found that the p21 protein levels (a marker of senescence) also increased under PM2.5 exposure (Figure 2(H,I)). These results validated that PM2.5 aggravated lung cellular senescence *in vitro* correlated with exposure dose and time.

3.3. PM2.5 triggers DNA damage and cGAS-STING pathway activation

Accumulation of DNA damage has been proved to be a key event of senescence (Li and Chen 2018). To assess the DNA damage caused by PM2.5 exposures, we investigated the ratio of γ H2AX foci formation, a marker of DNA DSBs. We quantified the fraction of fibroblasts positive to γ H2AX upon PM2.5 exposures, and notably, the results showed that PM2.5 caused increased γ H2AX-positive fibroblasts-significantly at 100 $\mu\text{g}/\text{mL}$ (Figure 3(A,B)). Accumulated DNA damages often trigger cGAS-STING pathway activation which is essential for cellular senescence (Pons et al. 2021; Wang et al. 2021). Upon the results of DNA damage caused by PM2.5, we assumed that PM2.5 would trigger cGAS activation. To verify whether the cellular senescence aggravated by PM2.5 is associated with cGAS-STING pathway, we detected the protein levels of cGAS and STING following PM2.5 exposure in fibroblasts. The results showed that PM2.5 caused upregulated protein levels of cGAS and STING (Figure 3(C,D)). The expression of cGAS was also upregulated around the pulmonary bronchi in the mice lung following the PM2.5 treatment at 5 mg/kg bw (Figure 3(F)). There is evidence that activated cGAS stimulates the production of cGAMP, which in turn causes STING to produce IFNs (Ablasser et al. 2013). To determine whether cGAS is activated, we detected the production of cGAMP with the ELISA kit and found that cGAMP production increased by approximately 2.5 times following PM2.5 exposures (Figure 3(E)). In addition, PM2.5 exposures also resulted in the upregulated transcription level of type I interferon IFI44 and ISG15 which were tightly correlated with cGAS activation and cellular senescence (Robin et al. 2014; Mackenzie et al. 2017;

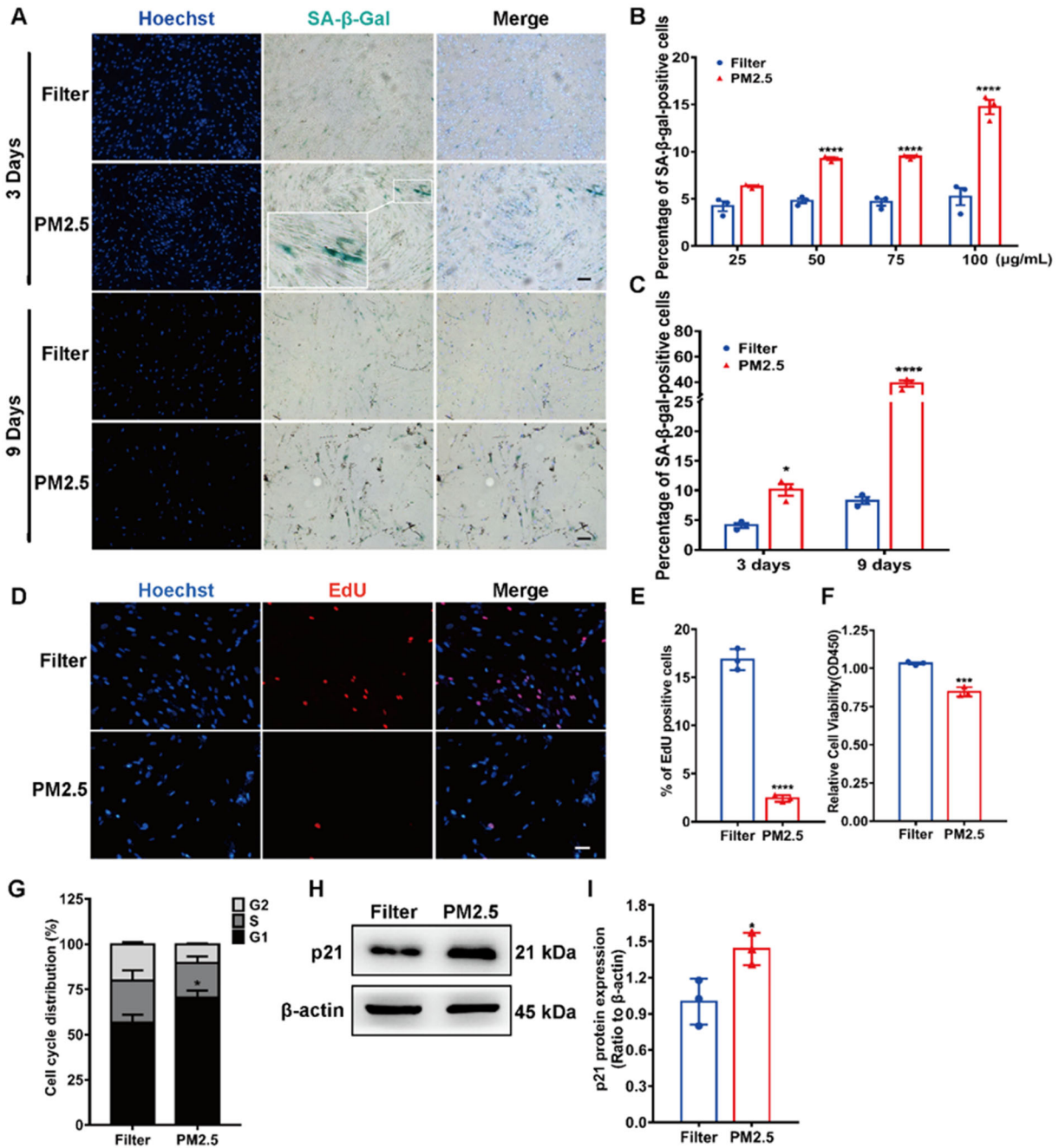


Figure 2. PM2.5 exposure induced lung fibroblasts senescence. (A) Representative images of senescent fibroblasts (blue) were detected with β -X-gal staining, Scale bar is 100 μ m. (B) Quantification of senescent fibroblasts with different concentrations of PM2.5 exposure. (C) Quantification of senescent fibroblasts at various time points post PM2.5 exposure. Two-way ANOVA followed by Student's t-test was used for time and dosage-dependent experiments. (D) Representative images of EdU assay, Scale bar is 100 μ m. (E) Quantification of cell proliferation determined by EdU assay at 100 μ g/mL for 3 d. (F) Cell viability of fibroblasts exposed to PM2.5 (100 μ g/mL for 3 d) was detected by CCK8. (G) Cell cycle of fibroblasts exposed to PM2.5 was analyzed by flow cytometry. (H) Protein levels of p21 in fibroblasts exposed to PM2.5 at 100 μ g/mL for 3 d. Beta-actin was loading control. (I) Quantification of p21 expression. Three independent experiments were processed. These data for in vivo experiment were represented as the mean \pm SD and in vitro for mean \pm SEM, * p < 0.05, *** p < 0.001, and **** p < 0.0001 compared with filter group by using Student's t-test.

Huijser et al. 2022; Figure 3(G,H)). It was reported that after the activation of cGAS-STING pathway, NF- κ B pathway can be activated, further causing some interleukin overexpression, such as IL1 β and

IL8 (Liao et al. 2020; Guo et al. 2021b). In our study, we quantified the gene transcription of IL1 β and IL8 after exposure to PM2.5. Notably, the gene expression level of IL-1 β and IL-8 in the lung

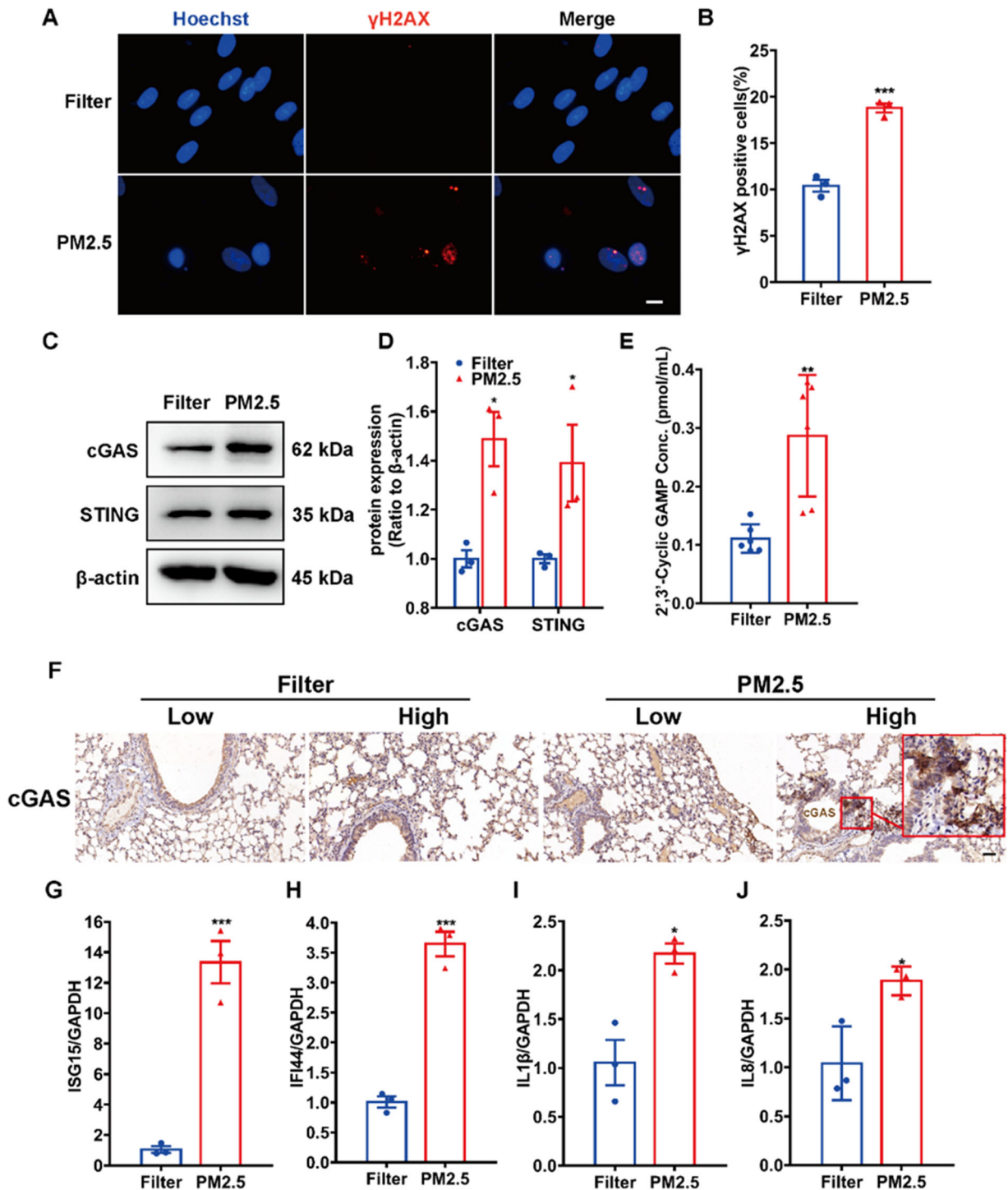


Figure 3. PM2.5 exposures induced DSBs and cGAS activation. Fibroblasts were exposed to PM2.5 at 100 μ g/mL for 3 d. (A) Representative images of immunofluorescence for γ H2AX following the exposure of PM2.5 and (B) Fraction of γ H2AX positive cells. Scale bar is 10 μ m. (C) Immunoblotting of cGAS and STING following the exposure of PM2.5. Beta-actin was loading control. (D) Quantification of cGAS and STING expression. (E) Production of cGAMP after PM2.5 exposures. (F) Histological examination of cGAS (brown) of mice lungs. Tissues sections were stained with Immunohistochemistry (IHC) (scale bar: 50 μ m). 'Low' and 'High' represent treatment concentrations of PM2.5 in mice of 1 and 5 mg/kg bw, respectively, $n = 4-5$ mice per group. (G, H) Relative gene expression changes of ISG15 and IFI44 following PM2.5 exposures. (I, J) Relative gene expression changes of IL1 β and IL8 following PM2.5 exposures. Three independent experiments were processed. These data are represented as the mean \pm SEM, * $p < 0.05$, ** $p < 0.01$, and *** $p < 0.001$ compared with filter group by using Student's t-test.

fibroblasts exposed to PM_{2.5} was higher than the filter group significantly (Figure 3(I,J)). These data demonstrated that PM_{2.5} exposure caused DNA damage and cGAS-STING pathway activation in fibroblasts.

3.4. PM_{2.5}-induced MN formation and cGAS gathered on MNs

HR and NHEJ are the main DNA repair pathway and the failure of DNA repair causes persistent DNA damage, which will result in increased MN formation (Feng et al. 2022). In addition, persistent DNA damage triggers signaling cascades that cause cell senescence (Swift, Sell, and Azizkhan-Clifford 2022). To test the effects of PM_{2.5} exposure on the HR and NHEJ repair efficiency, 293T cells containing reporters (Seluanov, Mao, and Gorbunova 2010) were exposed with PM_{2.5}. Compared with the filter group, PM_{2.5} exposures were found to significantly inhibit the DNA repair efficiency of HR but not NHEJ (Figure 4(A,B)). Moreover, PM_{2.5} exposure downregulated the protein level of Rad51 (Figure 4(C,D)), which was in coordination with the results of DNA repair efficiency. It was reported that persistent DNA damage promotes the MN formation closely (Paz et al. 2018; Clay et al. 2021). In this work, we determined that PM_{2.5} treatment led to the formation of a large number of MN (Figure 4(E,F)). In addition, not only in the primary nucleus, γ H2AX foci was also observed in ~80% MNs following PM_{2.5} exposures (Figure 4(G,H)). Activation of cGAS upon PM_{2.5} exposure was detected, but the trigger of cGAS activation was not clearly understood. To determine whether cGAS would gather in MN, GFP-cGAS-expressing fibroblasts were constructed and treated with PM_{2.5}. Consequently, we found that cGAS is localized to about 80% of MNs under PM_{2.5} exposure (Figure 4(I,J)). The results confirmed that PM_{2.5} exposure caused MNs formation and frequent localization of cGAS to MNs.

3.5. Rupture of nuclear envelope (NE) on MNs caused cGAS gathering

It was intriguing that although cGAS accumulated on the majority of MNs, there were few MNs without cGAS accumulation following PM_{2.5} exposures. To investigate the reason for the discrepancy, cGAS-

GFP-expressing fibroblasts were employed for the localization of cGAS under PM_{2.5} exposures and the nuclear membrane of fibroblasts were then labeled with a component of nuclear lamina, lamin A/C. The results showed that cGAS only localize to some MN with incomplete nuclear membrane which was characterized by one or several discontinuous holes in the nuclear membrane (Figure 5(A)). Although cGAS gathered in the majority of MNs with discontinuous nuclear rim of lamin A/C, some MNs with continuous nuclear rim accumulated cGAS as well. Further examination of another lamina component lamin B1 in fibroblasts subjected to PM_{2.5} exposures, surprisingly, revealed that almost all MNs with discontinuous nuclear rim of lamin B1 gathered cGAS (Figure 5(B,C)). Moreover, we co-stained the cells with lamin B1 and nuclear protein retinoblastoma (Rb), which was used for detecting integrity of nuclear envelopes (NEs). The results showed Rb only existed in MN with intact nuclear membrane in PM_{2.5}-exposed fibroblasts (Figure S1(A)).

In order to explore the discrepancy different nuclear lamina in cGAS localization to MNs, we co-stained fibroblasts with lamin A/C and lamin B1 under PM_{2.5} exposure. The results showed that some MNs exhibited continuous nuclear rim of lamin A/C but not lamin B1, and they did not exist in PM_{2.5}-exposed fibroblasts at the same time (Figure 6(A)). Statistical results demonstrated that MNs had a higher proportion of disrupted MN according to the labeled lamin B1, up to approximately 90%, than lamin A/C in PM_{2.5}-exposed fibroblasts (Figure 6(B,C)). Furthermore, we investigated the protein levels of lamin B1 and lamin A/C with western blotting, and found that PM_{2.5} exposure significantly decreased the protein level of lamin B1 (Figure 6(D,E)). Meanwhile, the protein level of lamin A and lamin C decrease rarely (Figure 6(D,E)). These data suggested that PM_{2.5}-induced MN disruption was correlated with lamina rupture in MNs, especially lamin B1.

3.6. Inhibition of cGAS decreased cellular senescence caused by PM_{2.5}

To further confirm whether cellular senescence induced by PM_{2.5} was caused by cGAS activation, we interfered cGAS expression with siRNA (10 nM) and the inhibition efficiency of cGAS by siRNA was

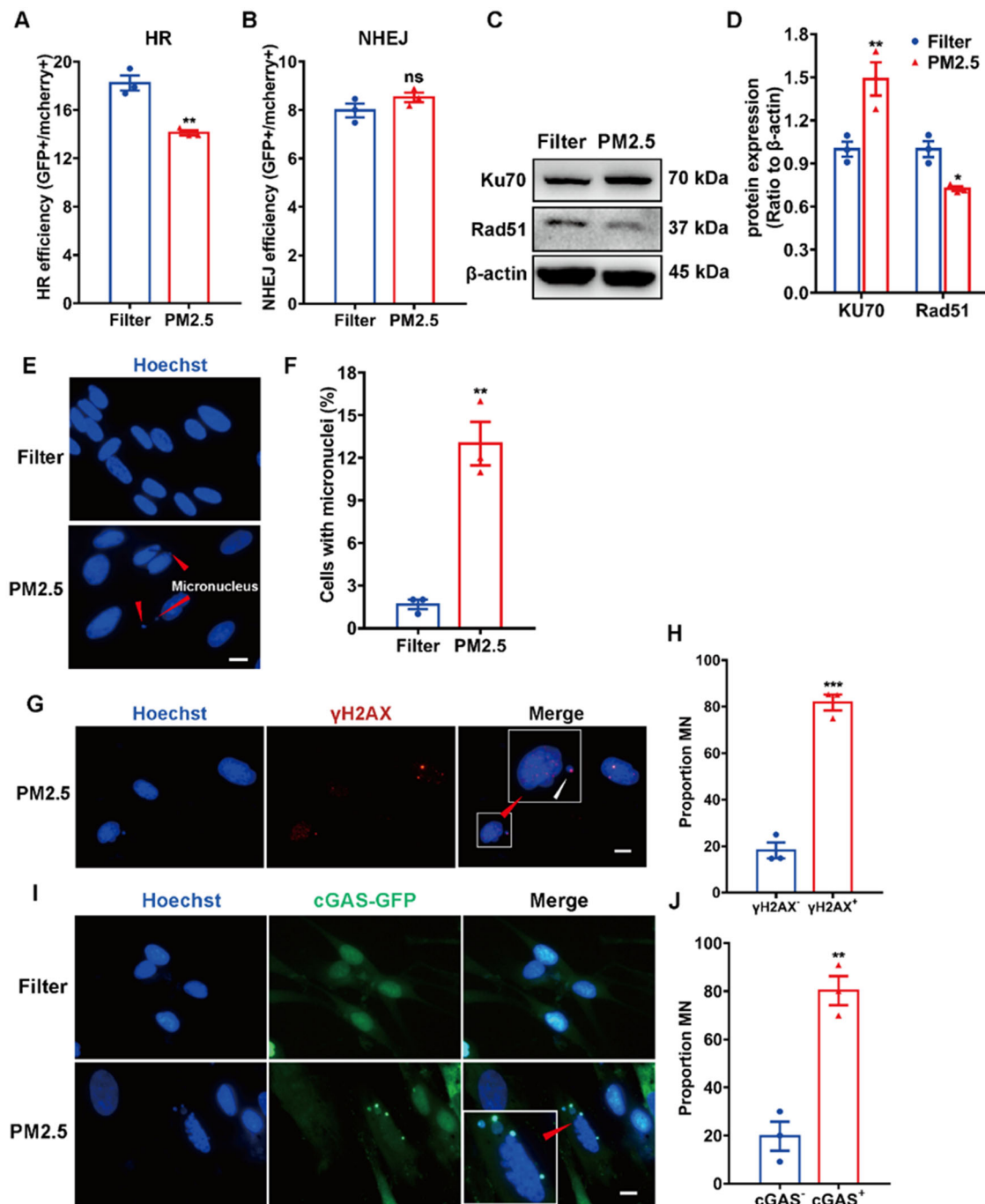


Figure 4. PM2.5 induced MN formation and cGAS gathered on MNs. Fibroblasts were exposed to PM2.5 (concentrations: 100 μ g/mL) for 3 d (Figure C–J). (A, B) Effect of PM2.5 exposures on the efficiency of HR and NHEJ in 293 T cells at 100 μ g/mL for 3 d. (C, D) Expression of Ku70 and Rad51 following exposures to PM2.5. Beta-actin was used as loading control. (E) Representative images of MNs after PM2.5 exposures and the nucleus were stained with Hoechst 33342. (F) MN formation rate was evaluated by the fluorescence microscope. (G) Immunofluorescence of γ H2AX in the MNs following the exposure to PM2.5. (H) Statistical analysis of the proportion of MNs with γ H2AX positive foci under treatment of PM2.5. (I) The localization of cGAS in cGAS-GFP-expressing HLF cells exposed to PM2.5. (J) Proportion of MNs containing cGAS-GFP was calculated statistically. Three independent experiments were processed. These data are represented as the mean \pm SEM, ns: not significant, * p < 0.05, ** p < 0.01, and *** p < 0.001 compared with filter group by using Student's t-test (Figure 4(A,B,F,H,J)) and two-way ANOVA (Figure 4(D)). Scale bar is 10 μ m.

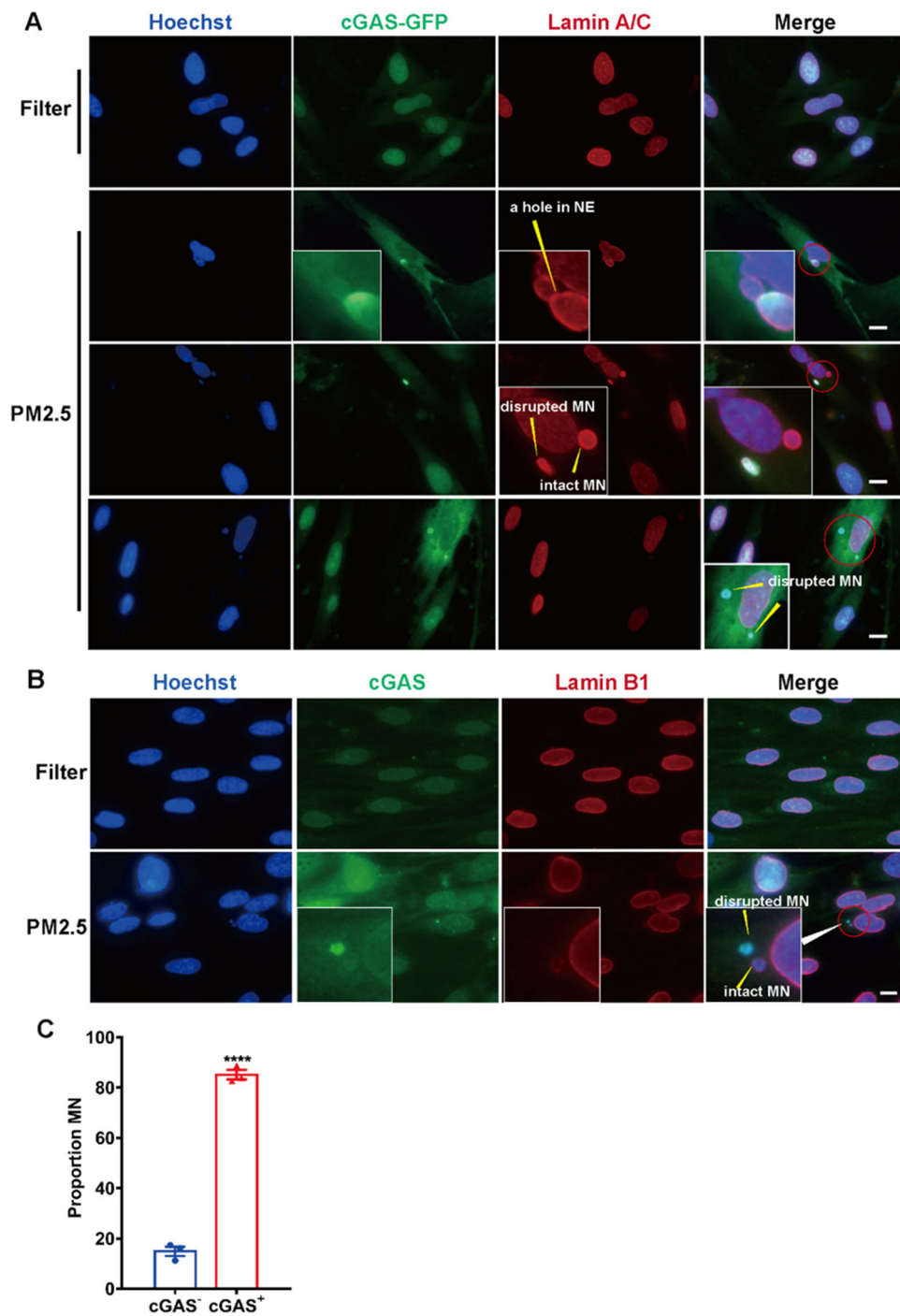


Figure 5. The localization of cGAS to MNs was associated with MN disruption. (A) cGAS-GFP expressing HLF cells were treated with PM2.5 for 3 d and MN membrane was labeled with lamin A/C. Scale bar was 10 μ m. (B) Fibroblasts exposed to PM2.5 (100 μ g/mL for 3 d) were co-stained with lamin B1 and cGAS. Scale bar is 10 μ m. (C) Proportion of MNs with anti-cGAS was calculated statistically. Three independent experiments were processed. These data are represented as the mean \pm SEM, **** p < 0.0001 compared with filter group by using Student's t-test.

detected (Figure S2(A,B)). The results indicated that cellular senescence was significantly reduced after cGAS inhibition in PM2.5-exposed fibroblasts (Figure 7(A,B)). Furthermore, we suppressed the cGAS enzyme activity with a small molecule selective inhibitor, Ru.521, which had been identified as a

selective inhibitor suppressing dsDNA-dependent activation of cGAS (Vincent et al. 2017). The activation of cGAS requires the involvement of dsDNA and Ru.521 suppresses cGAS activity by interfering with its association with dsDNA through binding to the catalytic pocket of cGAS competitively and

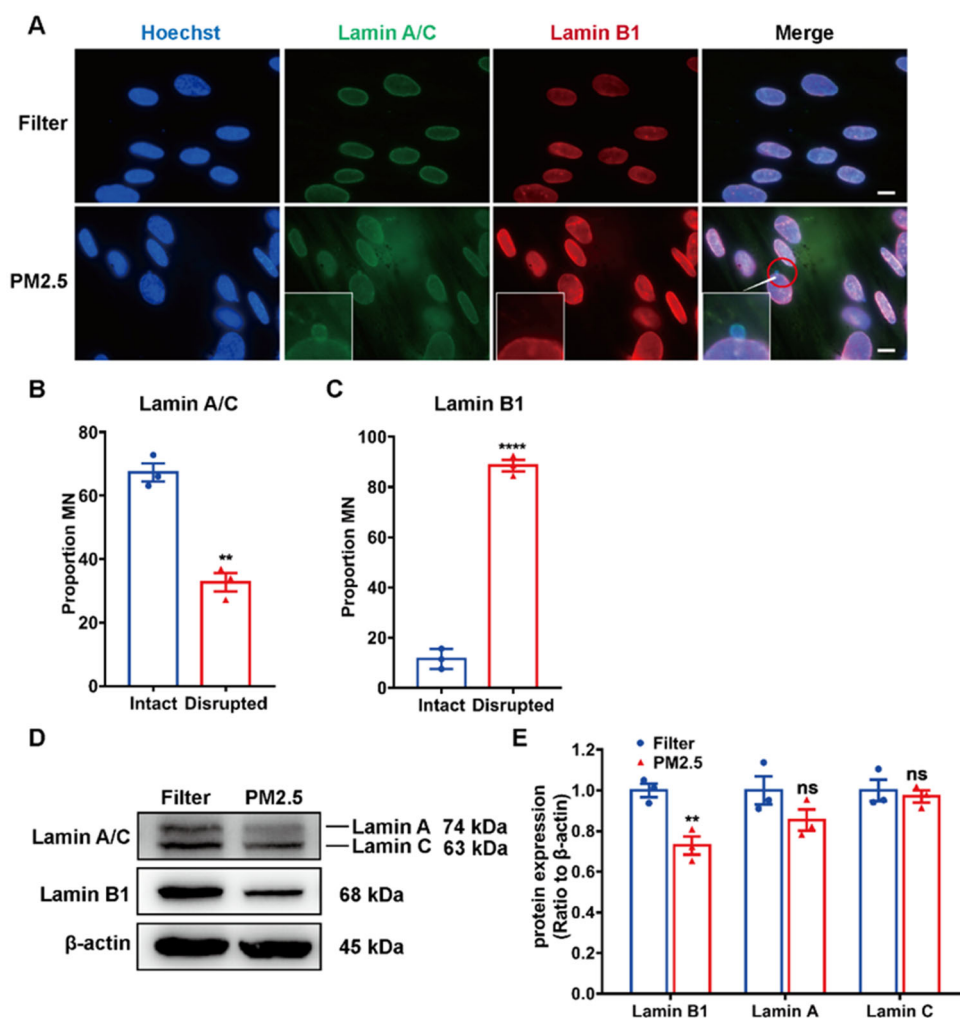


Figure 6. MNs disruption was related to lamin B1 downregulation. Fibroblasts were exposed to PM2.5 at 100 $\mu\text{g}/\text{mL}$ for 3 d. (A) Fibroblasts exposed to PM2.5 were co-stained with lamin A/C and lamin B1. Scale bar is 10 μm . (B, C) Proportion of intact and disrupted MN under PM2.5 exposures according to the labeled lamin B1 and lamin A/C. (D, E) Immunoblotting and quantification of lamin B1 and lamin A/C in fibroblasts treated with PM2.5. Three independent experiments were processed. These data are represented as the mean \pm SEM, ** $p < 0.01$ and **** $p < 0.0001$ compared with filter group by using Student's t-test and Two-way ANOVA (Figure E), ns: not significant.

inhibits its dsDNA-stimulated activity. As shown in Figure 7(C,D), cellular senescence induced by PM2.5 decreased significantly following treatment of Ru.521. In addition, we found that after knocking down the expression of cGAS by siRNA, the gene transcription levels of cGAS, ISG15, and IFI44 also decreased significantly (Figure 7(E–G)). Altogether, our findings demonstrated that PM2.5 caused cellular senescence in which cGAS played a key role.

4. Discussion

Epidemiological investigations demonstrated a close correlation between PM2.5 and respiratory diseases which were related to cellular senescence (Zhao

et al. 2019). However, whether PM2.5 causes cellular senescence is not yet fully understood from *in vitro* and *in vivo* studies. Using PM2.5 samples collected from Taiyuan, a coal hub in Northern China, we investigated the effects of PM2.5 exposures on cellular senescence both *in vivo* and *in vitro*.

Cellular senescence is a strengthening age-related process that contributes to senescence related diseases and is originally described as a persistent block of the cell cycle by Hayflick (Ogrodnik et al. 2019). Some respiratory diseases, such as IPF were found to be closely related to cellular senescence induced by cGAS activation in the clinic (Schuliga et al. 2020). In addition, pathological fibroblast populations involve cellular senescence, and

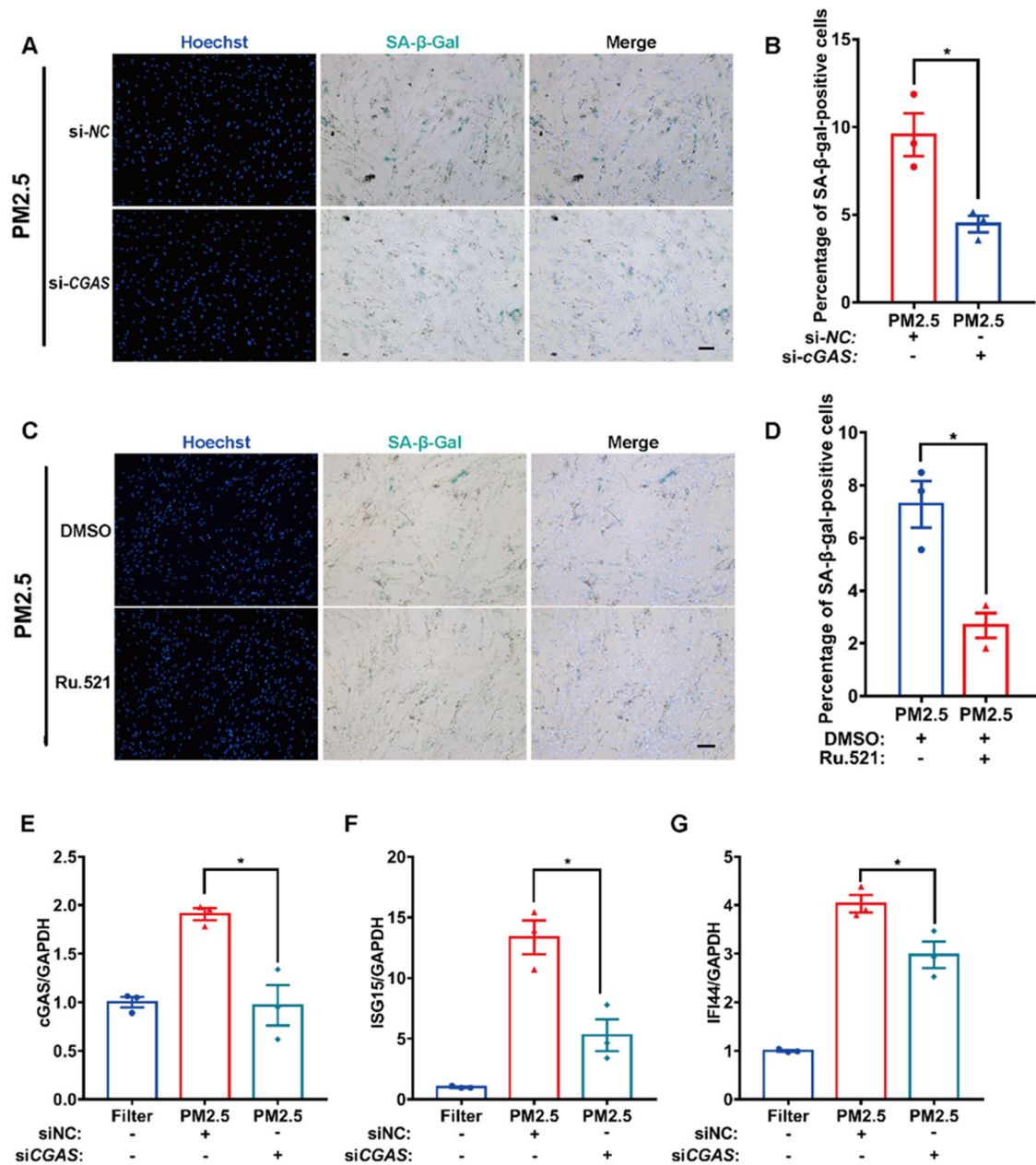


Figure 7. PM_{2.5}-stimulated senescence in fibroblasts in a cGAS-dependent manner. HLF cells were exposed to PM_{2.5} at 100 μg/mL for 3 d. (A) Cellular senescence caused by PM_{2.5} after knockdown of cGAS with β-X-gal staining. (B) Statistical analysis of the ratio of senescent cells with knockdown of cGAS. (C) Cellular senescence induced by PM_{2.5} after inhibition of cGAS enzyme activity by Ru.521 with β-X-gal staining. (D) Statistical analysis of the ratio of senescent cells with inhibition of cGAS enzyme activity. (E–G) Relative gene expression of cGAS, ISG15, and IFI44 in PM_{2.5}-exposed cells after knockdown of cGAS. Three independent experiments were processed. These data are represented as the mean ± SEM, **p* < 0.05 compared with filter group by using Student's t-test. Scale bar is 100 μm.

senescence modifies the release of many kinds of cytokines and growth factors in fibroblasts (Wu, Tang, and Kapoor 2021). Recent studies showed that an increase in senescence involving epigenetic regulatory mechanisms and mitochondrial damage upon PM_{2.5} exposure (Ryu et al. 2019; Herath et al. 2022). In this study, we determined that PM_{2.5} exposures aggravated cellular senescence elevated

by increased SA-β-gal activity *in vitro* in a time and dose dependent manner. To detect cellular senescence caused by PM_{2.5} *in vivo*, we treated mice with 1 and 5 mg/kg bw which simulated the environmental PM_{2.5} concentrations under normal and severely polluted conditions. Similarly, *in vivo* experimental results suggested that PM_{2.5} exposures aggravated cellular senescence in mice in a

dose dependent manner as well. Based on the above results, we confirmed that PM_{2.5} aggravate cellular senescence, involving the exposure time and dosage.

Though PM_{2.5} was found to aggravate cellular senescence, the particular mechanisms underlying were not clear. Aberrant activation of DNA damage response was demonstrated to result in MN formation and cell cycle arrest, leading to cellular senescence finally (Zhao et al. 2020). These results determined that PM_{2.5} exposures notably led to DSBs significantly. It was reported that cGAS is a DNA sensor that can be activated by environmental stimulates (Sharma et al. 2021). Considering the abundant DNA damages caused by PM_{2.5}, We assumed PM_{2.5} causes cGAS activation and detected the activation of cGAS upon PM_{2.5} exposures. Our results suggested that the cGAS and cGAMP were upregulated and increased, and the cGAS-STING pathway was triggered following by upregulation of IFI44 and ISG15 which were tightly correlated with cellular senescence. Through cGAS inhibition and suppression of the cGAS enzymic activity, we determined that PM_{2.5} exposures aggravated the senescence of fibroblasts in a cGAS dependent manner.

Nevertheless, we knew little about the specific causes of cGAS activation. It was reported that DNA fragments in MN could be recognized by cGAS accompanied with the activation of downstream inflammatory pathways (Mann and Kranzusch 2017). MN formation was generally thought to result from DSBs in which HR and NHEJ were important factors affecting DNA repair efficiency (Terradas, Martin, and Genesca 2016). We determined that PM_{2.5} treatment led to a large number of MN formation in which inhibition of HR repair efficiency by PM_{2.5} exposure played a vital role. Additionally, DNA damages were found in about 80% of MNs after PM_{2.5} exposures. DNA damages on MNs were reported to exacerbate micronucleus instability and DNA in the MN could be exposed to cytoplasm (Zhang et al. 2015). This led us to the conjecture that PM_{2.5} might induce MNs formation and that MNs were a potential source of immunostimulatory and cytosolic DNA to activate cGAS. To examine the localization of cGAS, we established GFP-cGAS-expressing HLF cells and exposed them to PM_{2.5}. Subsequently, cGAS was observed to gather in the

majority of MNs and the statistical results showed that about 80% of MNs accumulated cGAS. The results confirmed that MNs caused by PM_{2.5} exposures were the crucial source of cGAS.

It was puzzling that although cGAS accumulated on most MNs, there was no cGAS accumulation on a tiny minority of MNs following PM_{2.5} exposures. Research from a previous study demonstrated that NE rupture in primary nuclei was associated with disorganization in the nuclear lamina of cells (Hatch et al. 2013). According to the previous finding, those MNs gathered cGAS might have defects in the nuclear lamina assembly. To detect the integrity of lamina, we labeled cGAS and lamin A/C in fibroblasts exposed to PM_{2.5}, and found that although cGAS gathered in most MNs with the discontinuous nuclear rim of lamin A/C, indicating disruption of MNs, a few MNs with the continuous nuclear rim of lamin A/C still accumulated cGAS. Further labeling of lamin B1 showed that almost every MN with discontinuous nuclear rim of lamin B1 gathered cGAS. Co-staining of laminB1 and lamin A/C showed that MNs with continuous nuclear rim of lamin A/C presented discontinuous nuclear rim of lamin B1. Statistical results showed that both lamin B1 (about 90%) and lamin A/C (about 40%) had different degrees of rupture, and the rate of lamin B1 disorganization was closely related to the rate of cGAS gathering (about 80%). Consistent with the localization of lamina, the protein levels of lamin B1 decreased significantly and lamin A/C did not downregulate that much. Thus, we demonstrated that disrupted MNs were a source of cGAS activation to aggravate cellular senescence and lamin B1 triggered MNs disruption upon PM_{2.5} exposures.

In this study, we analyzed some metal element components of PM_{2.5}. The components of particle-bound chemicals change depending on emission sources, places, seasons, and climates (Li et al. 2022b). Numerous studies have indicated that the biological effects of PM are closely associated with heavy metals (Zhou et al. 2022). It was reported that Cr, As, and Pb were the major elements that contributed to the average non-carcinogenic risk, while Cr, As, and Cd were the elements with the highest carcinogenic risk (Li et al. 2022a). In addition, study showed that heavy metals significantly induced cellular senescence with activation of NF-kappa B pathway and mitochondrial dysfunction

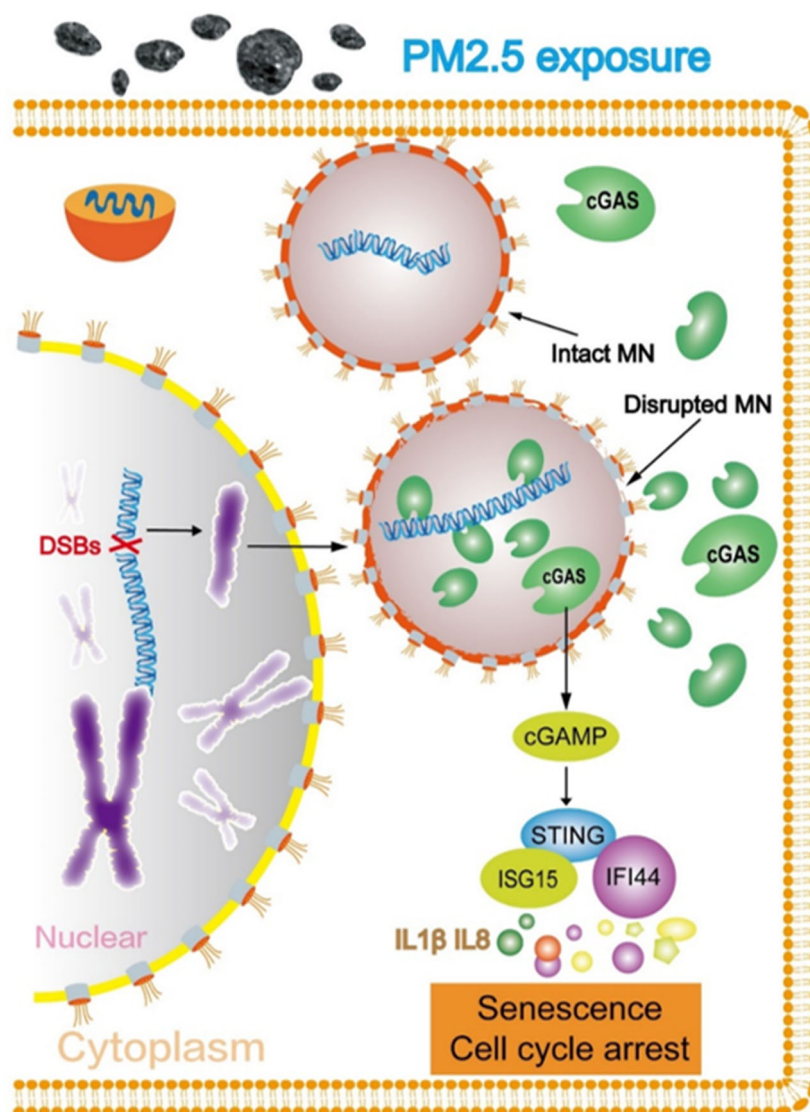


Figure 8. The schematic diagram of PM2.5-induced cellular senescence by MN disruption and cGAS-STING pathway activation. PM2.5 caused DNA DSBs and MNs formation. Following the formation of MNs, the nuclear membrane of some MNs disrupted under PM2.5 exposure and cGAS localize to the disrupted MNs. Subsequently, cGAS-STING pathway was activated and cellular senescence is induced in PM2.5-exposed fibroblasts.

(Luo et al. 2021). In our investigation, high levels of heavy metals (such as Mn, Cr, As, and Pb) were found in the PM2.5 samples, which may be the major factor of its cytotoxicity in cell senescence and the combinations of different heavy metals content deserve further study for the accurate toxicity of PM2.5 components.

5. Conclusion

In conclusion, this study confirmed that PM2.5 exposures aggravated lung cellular senescence depending on the cGAS-STING pathway activation,

which typically involves recognition of disrupted MNs by cGAS (Figure 8). Different from the previous studies, PM2.5-induced senescence in our study involved the recognition of self-DNA and triggered autoimmune activities through cGAS activation. The findings provided new insights into understanding the potential toxicity of PM2.5 and a novel mechanism in PM2.5-induced cellular senescence.

Ethics approval

Ethical approval was given by the Institutional Animal Care and Use Committee of Hefei Institutes of Physical Science,

Chinese Academy of Sciences (Reference number: SWYX-Y-2021-10) for isolation of fibroblasts. Informed consent was obtained. All mice in the study were allowed free access to water and food and all procedures were approved by the Institutional Animal Care and Use Committee of Hefei Institutes of Physical Science, Chinese Academy of Sciences (Laboratory Animal Facility License Number: SYXK-2019-010). All animals were treated humanely in accordance with the National Institutes of Health Guide for the Care and Use of Laboratory Animals.

Acknowledgments

The authors thank Prof. Sang for giving PM2.5 sample. The original NHEJ and HR Reporter was a gift from Dr. Gorbunova. A portion of the work was performed on the Steady High Magnetic Field Facilities, CAS and supported by the High Magnetic Field Laboratory of Anhui Province' should be 'The work was performed on the High Magnetic Field Laboratory of Anhui Province.

Disclosure statement

The authors report there are no competing interests to declare.

Authorship statement

Performed research: W.T., C.B., B.L., and M.J.; Conceived of study: W.T.; Analyzed data: W.T., H.W., X.S.; Designed study: X.A., W.L., and C.S.; Wrote the article: K.N. Yu, W.L., C.S.

Funding

The work was supported by NSFC Regional Innovation and Development Joint Fund (U22A20406), the Key Program of 13th five-year plan, CASHIPS (No. KP-2017-05), and Anhui Provincial Natural Science Foundation (2108085MB41 and 2008085MC66).

ORCID

Biao Chen  <http://orcid.org/0000-0003-4837-9104>
Shaopeng Chen  <http://orcid.org/0000-0002-3632-9727>

References

- Abbas, I., G. Garçon, F. Saint-Georges, V. Andre, P. Gosset, S. Billet, J. Le Goff, A. Verdin, et al. 2013. "Polycyclic Aromatic Hydrocarbons within Airborne Particulate Matter (PM2.5) Produced DNA Bulky Stable Adducts in a Human Lung Cell Coculture Model." *Journal of Applied Toxicology* 33 (2): 109–119. <http://dx.doi.org/10.1002/jat.1722>.
- Ablasser, A., M. Goldeck, T. Cavlar, T. Deimling, G. Witte, I. Rohl, K. P. Hopfner, J. Ludwig, et al. 2013. "cGAS Produces a 2'-5'-Linked Cyclic Dinucleotide Second Messenger That Activates STING." *Nature* 498 (7454): 380–384. <http://dx.doi.org/10.1038/nature12306>.
- Araviiskaia, E., E. Berardesca, T. Bieber, G. Gontijo, M. S. Viera, L. Marrot, B. Chuberre, and B. Dreno. 2019. "The Impact of Airborne Pollution on Skin." *Journal of the European Academy of Dermatology and Venereology* 33 (8): 1496–1505. <http://dx.doi.org/10.1111/jdv.15583>.
- Baker, D. J., B. G. Childs, M. Durik, M. E. Wijers, C. J. Sieben, J. Zhong, R. A. Saltness, K. B. Jeganathan, et al. 2016. "Naturally Occurring p16(Ink4a)-Positive Cells Shorten Healthy Lifespan." *Nature* 530 (7589): 184–189. <http://dx.doi.org/10.1038/nature16932>.
- Childs, B. G., D. J. Baker, T. Wijshake, C. A. Conover, J. Campisi, and J. M. Van Deursen. 2016. "Senescent Intimal Foam Cells Are Deleterious at All Stages of Atherosclerosis." *Science* 354 (6311): 472–477. <http://dx.doi.org/10.1126/science.aaf6659>.
- Clay, D. E., H. S. Bretscher, E. A. Jezuit, K. B. Bush, and D. T. Fox. 2021. "Persistent DNA Damage Signaling and DNA Polymerase Theta Promote Broken Chromosome Segregation." *Journal of Cell Biology* 220 (12): e202106116. <http://dx.doi.org/10.1083/jcb.202106116>.
- Demaria, M., M. N. O'leary, J. H. Chang, L. J. Shao, S. Liu, F. Alimirah, K. Koenig, C. Le, et al. 2017. "Cellular Senescence Promotes Adverse Effects of Chemotherapy and Cancer Relapse." *Cancer Discovery* 7 (2): 165–176. <http://dx.doi.org/10.1158/2159-8290.Cd-16-0241>.
- Di Domenico, M., S. G. D. Benevenuto, P. P. Tomasini, V. Y. Yariwake, N. D. Alves, F. L. Rahmeier, M. D. Fernandes, D. J. Moura, et al. 2020. "Concentrated Ambient Fine Particulate Matter (PM2.5) Exposure Induce Brain Damage in Pre and Postnatal Exposed Mice." *Neurotoxicology* 79: 127–141. <http://dx.doi.org/10.1016/j.neuro.2020.05.004>.
- Feng, Y. L., Q. Liu, R. D. Chen, S. C. Liu, Z. C. Huang, K. M. Liu, X. Y. Yang, and A. Y. Xie. 2022. "DNA Nicks Induce Mutational Signatures Associated with BRCA1 Deficiency." *Nature Communications* 13 (1): 4285. <http://dx.doi.org/10.1038/s41467-022-32011-x>.
- Forouzanfar, M. H., A. Afshin, L. T. Alexander, H. R. Anderson, Z. A. Bhutta, S. Biryukov, M. Brauer, R. Burnett, et al. 2016. "Global, Regional, and National Comparative Risk Assessment of 79 Behavioural, Environmental and Occupational, and Metabolic Risks or Clusters of Risks, 1990–2015: A Systematic Analysis for the Global Burden of Disease Study 2015." *The Lancet* 388 (10053): 1659–1724. [http://dx.doi.org/10.1016/S0140-6736\(16\)31679-8](http://dx.doi.org/10.1016/S0140-6736(16)31679-8).
- Guo, Q., X. Chen, J. Chen, G. Zheng, C. Xie, H. Wu, Z. Miao, Y. Lin, et al. 2021b. "STING Promotes Senescence, Apoptosis, and Extracellular Matrix Degradation in Osteoarthritis via the NF-kappaB Signaling Pathway." *Cell Death & Disease* 12 (1): 13. <http://dx.doi.org/10.1038/s41419-020-03341-9>.
- Hatch, E. M., A. H. Fischer, T. J. Deerinck, and M. W. Hetzer. 2013. "Catastrophic Nuclear Envelope Collapse in Cancer Cell Micronuclei." *Cell* 154 (1): 47–60. <http://dx.doi.org/10.1016/j.cell.2013.06.007>.

- Herath, M. U. L. H., M. J. Piao, K. A. Kang, A. X. Zhen, P. D. S. M. Fernando, H. K. Kang, J. M. Yi, and, J. W. Hyun. 2022. "Hesperidin Exhibits Protective Effects against PM2.5-Mediated Mitochondrial Damage, Cell Cycle Arrest, and Cellular Senescence in Human HaCaT Keratinocytes." *Molecules* 27 (15): 4800. <http://dx.doi.org/10.3390/molecules27154800>
- Hintzsche, H., U. Hemmann, A. Poth, D. Utesch, J. Lott, and H. Stopper, Working Group "In vitro micronucleus test", Gesellschaft für Umwelt-Mutationsforschung (GUM, German-speaking section of the European Environmental Mutagenesis and Genomics Society EEMGS). 2017. "Fate of Micronuclei and Micronucleated Cells." *Mutation Research. Reviews in Mutation Research* 771: 85–98. <http://dx.doi.org/10.1016/j.mrrev.2017.02.002>.
- Huijser, E., I. L. A. Bodewes, M. S. Lourens, C. G. van Helden-Meeuwse, T. P. P. van den Bosch, D. G. B. Grashof, H. J. G. van de Werken, et al. 2022. "Hyperresponsive Cytosolic DNA-Sensing Pathway in Monocytes from Primary Sjogren's Syndrome." *Rheumatology* 61 (8): 3491–3496. <http://dx.doi.org/10.1093/rheumatology/keac016>
- Kamal, N. S. M., S. Safuan, S. Shamsuddin, and P. Foroozandeh. 2020. "Aging of the Cells: Insight into Cellular Senescence and Detection Methods." *European Journal of Cell Biology* 99 (6): 151108. <http://dx.doi.org/10.1016/j.ejcb.2020.151108>.
- Li, L., R. Meng, Y. L. Lei, S. M. Wu, and Y. Jiang. 2022a. "Human Health Risk Assessment of Heavy Metals from PM2.5 in China's 29 Provincial Capital Cities." *Environmental Science and Pollution Research* 29: 63028–63040. <http://dx.doi.org/10.1007/s11356-022-20229-7>
- Li, T., and Z. J. Chen. 2018. "The cGAS-cGAMP-STING Pathway Connects DNA Damage to Inflammation, Senescence, and Cancer." *The Journal of Experimental Medicine* 215 (5): 1287–1299. <http://dx.doi.org/10.1084/jem.20180139>.
- Li, X., C. Yan, C. Wang, J. Ma, W. Li, J. Liu, and Y. Liu. 2022b. "PM2.5-Bound Elements in Hebei Province, China: Pollution Levels, Source Apportionment and Health Risks." *The Science of the Total Environment* 806 (Pt 1): 150440. <http://dx.doi.org/10.1016/j.scitotenv.2021.150440>.
- Liao, Y., J. Cheng, X. Kong, S. Li, X. Li, M. Zhang, H. Zhang, et al. 2020. "HDAC3 Inhibition Ameliorates Ischemia/Reperfusion-Induced Brain Injury by Regulating the Microglial cGAS-STING Pathway." *Theranostics* 10 (21): 9644–9662. <http://dx.doi.org/10.7150/thno.47651>.
- Longhin, E., J. A. Holme, K. B. Gutzkow, V. M. Arlt, J. E. Kucab, M. Camatini, and M. Gualtieri. 2013. "Cell Cycle Alterations Induced by Urban PM2.5 in Bronchial Epithelial Cells: Characterization of the Process and Possible Mechanisms Involved." *Particle and Fibre Toxicology* 10: 63. <http://dx.doi.org/10.1186/1743-8977-10-63>.
- Luo, H. G., R. J. Gu, H. Y. Ouyang, L. H. Wang, S. W. Shi, Y. N. Ji, B. C. Bao, G. Q. Liao, et al. 2021. "Cadmium Exposure Induces Osteoporosis through Cellular Senescence, Associated with Activation of NF-Kappa B Pathway and Mitochondrial Dysfunction." *Environmental Pollution (Barking, Essex: 1987)* 290: 118043. <http://dx.doi.org/10.1016/j.envpol.2021.118043>.
- Mackenzie, K. J., P. Carroll, C. A. Martin, O. Murina, A. Fluteau, D. J. S. Impson, N. Olova, H. Sutcliffe, et al. 2017. "cGAS Surveillance of Micronuclei Links Genome Instability to Innate Immunity." *Nature* 548 (7668): 461–465. <http://dx.doi.org/10.1038/nature23449>
- Mann, C. C. D., and P. J. Kranzusch. 2017. "cGAS Conducts Micronuclei DNA Surveillance." *Trends in Cell Biology* 27 (10): 697–698. <http://dx.doi.org/10.1016/j.tcb.2017.08.007>.
- Ogrodnik, M., H. Salmonowicz, D. Jurk, and J. F. Passos. 2019. "Expansion and Cell-Cycle Arrest: Common Denominators of Cellular Senescence." *Trends in Biochemical Sciences* 44 (12): 996–1008. <http://dx.doi.org/10.1016/j.tibs.2019.06.011>.
- Paz, M. F. C. J., A. L. P. Sobral, J. N. Picada, I. Grivicich, A. L. Gomes, A. M. O. F. Da Mata, M. V. O. B. De Alencar, R. M. De Carvalho, et al. 2018. "Persistent Increased Frequency of Genomic Instability in Women Diagnosed with Breast Cancer: Before, during, and after Treatments." *Oxidative Medicine and Cellular Longevity* 2018: 2846819. <http://dx.doi.org/10.1155/2018/2846819>.
- Peng, F., G. Tsuji, J. Z. Zhang, Z. Chen, and M. Furue. 2019. "Potential Role of PM2.5 in Melanogenesis." *Environment International* 132: 105063. <http://dx.doi.org/10.1016/j.envint.2019.105063>.
- Pons, B. J., A. Pettes-Duler, C. Naylies, F. Taieb, C. Bouchenot, S. Hashim, P. Rouimi, M. Deslande, et al. 2021. "Chronic Exposure to Cytolethal Distending Toxin (CDT) Promotes a cGAS-Dependent Type I Interferon Response." *Cellular and Molecular Life Sciences* 78 (17–18): 6319–6335. <http://dx.doi.org/10.1007/s00018-021-03902-x>
- Robin, J. D., A. T. Ludlow, K. Batten, F. Magdinier, G. Stadler, K. R. Wagner, J. W. Shay, and W. E. Wright. 2014. "Telomere Position Effect: Regulation of Gene Expression with Progressive Telomere Shortening over Long Distances." *Genes & Development* 28 (22): 2464–2476. <http://dx.doi.org/10.1101/gad.251041.114>.
- Ryu, Y. S., K. A. Kang, M. J. Piao, M. J. Ahn, J. M. Yi, S. G. Bossi, Y. M. Hyun, C. O. Park, et al. 2019. "Particulate Matter-Induced Senescence of Skin Keratinocytes Involves Oxidative Stress-Dependent Epigenetic Modifications." *Experimental & Molecular Medicine* 51 (9): 1–14. <http://dx.doi.org/10.1038/s12276-019-0305-4>.
- Schuliga, M., J. Read, K. E. C. Blokland, D. W. Waters, J. Burgess, C. Prele, S. E. Mutsaers, J. Jaffar, et al. 2020. "Self DNA Perpetuates IPF Lung Fibroblast Senescence in a cGAS-Dependent Manner." *Clinical Science (London, England: 1979)* 134 (7): 889–905. <http://dx.doi.org/10.1042/Cs20191160>.
- Seluanov, A., C. Hine, M. Bozzella, A. Hall, T. H. C. Sasahara, A. aCM Ribeiro, K. C. Catania, D. C. Presgraves, et al. 2008. "Distinct Tumor Suppressor Mechanisms Evolve in Rodent Species That Differ in Size and Lifespan." *Aging Cell* 7 (6): 813–823. <http://dx.doi.org/10.1111/j.1474-9726.2008.00431.x>.

- Seluanov, A., Z. Mao, and V. Gorbunova. 2010. "Analysis of DNA Double-Strand Break (DSB) Repair in Mammalian Cells." *Journal of Visualized Experiments* 8: 2002. <http://dx.doi.org/10.3791/2002>
- Sharma, J., K. Parsai, P. Raghuwanshi, S. A. Ali, V. Tiwari, A. Bhargava, and P. K. Mishra. 2021. "Emerging Role of Mitochondria in Airborne Particulate Matter-Induced Immunotoxicity." *Environmental Pollution (Barking, Essex: 1987)* 270: 116242. <http://dx.doi.org/10.1016/j.envpol.2020.116242>
- Song, X. Y., J. H. Liu, N. B. Geng, Y. C. Shan, B. Q. Zhang, B. F. Zhao, Y. W. Ni, et al. 2022. "Multi-Omics Analysis to Reveal Disorders of Cell Metabolism and Integrin Signaling Pathways Induced by PM2.5." *Journal of Hazardous Materials* 424 (Pt C): 127573. <http://dx.doi.org/10.1016/j.jhazmat.2021.127573>
- Swift, M. L., C. Sell, and J. Azizkhan-Clifford. 2022. "DNA Damage-Induced Degradation of Sp1 Promotes Cellular Senescence." *GeroScience* 44 (2): 683–698. <http://dx.doi.org/10.1007/s11357-021-00456-5>
- Tahara, M., Y. Fujino, K. Yamasaki, K. Oda, T. Kido, N. Sakamoto, T. Kawanami, K. Kataoka, et al. 2021. "Exposure to PM2.5 is a Risk Factor for Acute Exacerbation of Surgically Diagnosed Idiopathic Pulmonary Fibrosis: A Case-Control Study." *Respiratory Research* 22 (1): 80. <http://dx.doi.org/10.1186/s12931-021-01671-6>
- Terradas, M., M. Martin, and A. Genesca. 2016. "Impaired Nuclear Functions in Micronuclei Results in Genome Instability and Chromothripsis." *Archives of Toxicology* 90 (11): 2657–2667. <http://dx.doi.org/10.1007/s00204-016-1818-4>
- Van Deursen, J. M. 2014. "The Role of Senescent Cells in Ageing." *Nature* 509 (7501): 439–446. <http://dx.doi.org/10.1038/nature13193>
- Vincent, J., C. Adura, P. Gao, A. Luz, L. Lama, Y. Asano, R. Okamoto, T. Imaeda, et al. 2017. "Small Molecule Inhibition of cGAS Reduces Interferon Expression in Primary Macrophages from Autoimmune Mice." *Nature Communications* 8 (1): 750. <http://dx.doi.org/10.1038/s41467-017-00833-9>
- Wang, C., Z. Y. Sun, C. X. Zhao, Z. W. Zhang, H. R. Wang, Y. Liu, Y. F. Guo, B. T. Zhang, et al. 2021. "Maintaining Manganese in Tumor to Activate cGAS-STING Pathway Evokes a Robust Abscopal anti-Tumor Effect." *Journal of Controlled Release: Official Journal of the Controlled Release Society* 331: 480–490. <http://dx.doi.org/10.1016/j.jconrel.2021.01.036>
- Wang, W. J., X. M. Chen, and G. Y. Cai. 2021. "Cellular Senescence and the Senescence-Associated Secretory Phenotype: Potential Therapeutic Targets for Renal Fibrosis." *Experimental Gerontology* 151: 111403. <http://dx.doi.org/10.1016/j.exger.2021.111403>
- Wang, Z., L. M. Ma, M. Q. Su, Y. R. Zhou, K. Mao, C. Q. Li, G. Y. Peng, et al. 2018. "Baicalin Induces Cellular Senescence in Human Colon Cancer Cells via Upregulation of DEPP and the Activation of Ras/Raf/MEK/ERK Signaling." *Cell Death & Disease* 9: 217. <http://dx.doi.org/10.1038/s41419-017-0223-0>
- Wu, B., L. Tang, and M. Kapoor. 2021. "Fibroblasts and Their Responses to Chronic Injury in Pulmonary Fibrosis." *Seminars in Arthritis and Rheumatism* 51 (1): 310–317. <http://dx.doi.org/10.1016/j.semarthrit.2020.12.003>
- Yang, H., H. Z. Wang, J. Y. Ren, Q. Chen, and Z. J. J. Chen. 2017. "cGAS is Essential for Cellular Senescence." *Proceedings of the National Academy of Sciences of the United States of America* 114 (23): E4612–E4620. <http://dx.doi.org/10.1073/pnas.1705499114>
- Yang, L., C. Li, and X. Tang. 2020. "The Impact of PM2.5 on the Host Defense of Respiratory System." *Frontiers in Cell and Developmental Biology* 8: 91. <http://dx.doi.org/10.3389/fcell.2020.00091>
- Zhang, C. Z., A. Spektor, H. Cornils, J. M. Francis, E. K. Jackson, S. W. Liu, M. Meyerson, and D. Pellman. 2015. "Chromothripsis from DNA Damage in Micronuclei." *Nature* 522 (7555): 179–184. <http://dx.doi.org/10.1038/nature14493>
- Zhao, J. L., M. Li, Z. H. Wang, J. K. Chen, J. P. Zhao, Y. J. Xu, X. Wei, et al. 2019. "Role of PM2.5 in the Development and Progression of COPD and Its Mechanisms." *Respiratory Research* 20 (1): 120. <http://dx.doi.org/10.1186/s12931-019-1081-3>
- Zhao, Z., Q. Dong, X. Liu, L. Wei, L. Liu, Y. Li, and X. Wang. 2020. "Dynamic Transcriptome Profiling in DNA Damage-Induced Cellular Senescence and Transient Cell-Cycle Arrest." *Genomics* 112 (2): 1309–1317. <http://dx.doi.org/10.1016/j.ygeno.2019.07.020>
- Zhou, Q., J. Chen, J. Zhang, F. Zhou, J. Zhao, X. Wei, K. Zheng, J. Wu, B. Li, and B. Pan. 2022. "Toxicity and Endocrine-Disrupting Potential of PM2.5: Association with Particulate Polycyclic Aromatic Hydrocarbons, Phthalate Esters, and Heavy Metals." *Environmental Pollution (Barking, Essex: 1987)* 292 (Pt A): 118349. <http://dx.doi.org/10.1016/j.envpol.2021.118349>